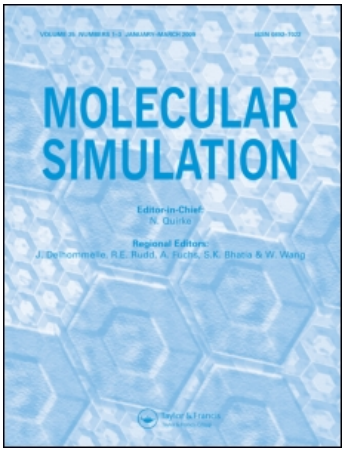

Molecular Simulation
Publication details, including instructions for authors and subscription information:
http://www.informaworld.com/smpp/title~content=t713644482

Molecular dynamics simulation and experimental validation of the effect of pH on protein desorption in hydrophobic charge induction chromatography

Lin Zhang[a]; Guofeng Zhao[a]; Yan Sun[a]
[a] Department of Biochemical Engineering, School of Chemical Engineering and Technology, Tianjin University, Tianjin, P.R. China

Online publication date: 24 November 2010

To cite this Article Zhang, Lin , Zhao, Guofeng and Sun, Yan(2010) 'Molecular dynamics simulation and experimental validation of the effect of pH on protein desorption in hydrophobic charge induction chromatography', Molecular Simulation, 36: 13, 1096 — 1103
To link to this Article: DOI: 10.1080/08927022.2010.506511
URL: http://dx.doi.org/10.1080/08927022.2010.506511

Molecular Simulation
Vol. 36, No. 13, November 2010, 1096–1103

Taylor & Francis
Taylor & Francis Group

Molecular dynamics simulation and experimental validation of the effect of pH on protein desorption in hydrophobic charge induction chromatography

Lin Zhang, Guofeng Zhao and Yan Sun*

Department of Biochemical Engineering, School of Chemical Engineering and Technology, Tianjin University, Tianjin 300072, P.R. China

(*Received 28 February 2010; final version received 2 July 2010*)

The ligands in hydrophobic charge induction chromatography (HCIC) are hydrophobic and ionisable. Thus, the pH is crucial for the separation performance in HCIC, especially for elution. However, it is difficult to obtain the microscopic information in HCIC through experimental means. In this work, molecular dynamics simulations are performed to examine the effect of pH on elution and protein conformational transition in HCIC, using a 46-bead β-barrel coarse-grained model protein and an HCIC adsorbent pore model constructed in an earlier work. Corresponding experiments are carried out for the validation of simulation results, using lysozyme and MEP Hypercel. Both the activities and fluorescence of lysozyme are examined to evaluate the conformational transition. The simulations indicate that the elution efficiency of protein increases with decreasing pH value in a non-linear manner. This is qualitatively consistent with the experimental results. MD simulations indicate that protein unfolding occurs in elution at all pH values. However, the experimental data show that the activity and conformation of lysozyme is independent of pH of the elution buffer. The microscopic information from simulation shows that protein unfolding is mainly observed on the adsorbent surface, but it cannot be detected in the experiments that only probe the proteins in the bulk liquid.

Keywords: molecular dynamics simulation; hydrophobic charge induction chromatography; elution; lysozyme; protein unfolding

Nomenclature

B	stably bound state of protein
d	the minimum distance between the protein and ligands
D	dissociated state of protein
E	inter-molecular interaction energy between the protein and ligands
f	mole fraction
M	intermediate state of protein
M_T	total number of trajectories
N	native state of protein
$P_{D,sim}$	the desorption probability from simulation
$P_{D,exp}$	the elution efficiency in experiment
R_g	radius of gyration of protein
U	unfolded state of protein
χ	structural overlap function

1. Introduction

Hydrophobic charge induction chromatography (HCIC) is an improved mode of hydrophobic interaction chromatography (HIC) firstly proposed by Burton and Harding [1]. Its ligands contain both hydrophobic and ionisable groups. As with HIC, protein can be adsorbed onto the ligands at neutral pH by hydrophobic interactions. The elution is, however, different from HIC. In HIC, elution is promoted by reducing salt concentration, while in HCIC, elution is promoted by electrostatic repulsion. By appropriately reducing the pH of the mobile phase below the pK_a of ligands and the isoelectric point of protein, both the ligands and protein can carry positive charges to obtain complete desorption of captured proteins. HCIC has many advantages, such as moderate operation condition, high adsorption capacity and easy elution of bound protein. Its separation performance has been verified on antibodies [1–7] and various other proteins [4,8–11]. The research on HCIC behaviours is important for bioseparation, and thus for the downstream processes of recombinant proteins.

As mentioned above, the pH of the mobile phase is very important for the adsorption and elution in HCIC. At neutral pH, ligands can attract the protein by hydrophobic interaction. After properly reducing the pH, ligands can repulse away the protein by electrostatic repulsion. Therefore, different pH of the mobile phase changes the driving force between the protein and ligands, and then promotes adsorption or desorption. Moreover, protein conformation and its activity may be dependent on the pH. So, the effect of pH in HCIC should be elucidated, especially, for the elution and conformational transition. However, it is difficult to examine the micro-process in the adsorbent pores experimentally. The understanding about protein adsorption, elution and conformational transition within the adsorbent pores is far from adequate.

*Corresponding author. Email: ysun@tju.edu.cn

ISSN 0892-7022 print/ISSN 1029-0435 online

DOI: 10.1080/08927022.2010.506511
http://www.informaworld.com

Molecular dynamics simulation focuses on small scales of time and space [12]. It can provide the details at the molecular level, and has been successfully utilised to investigate the adsorption phenomena and related chromatographic processes [13–20], as well as the protein conformational transition [21–23]. In previous simulations [24], a coarse-grained adsorbent pore model has been proposed to explore the molecular insight into the protein conformational transition within adsorbent pores. In the present study, the charge number carried in the ligands is adjusted to simulate different pH of the mobile phase. The effect of pH is then investigated by molecular dynamics simulations, using a 46-bead β-barrel coarse-grained model protein within the pores at various pH values (3–7). The elution efficiency and native fraction of the protein are calculated from the simulation results. After that, finite batch adsorption experiments are performed using lysozyme and a commercial HCIC adsorbent, MEP (4-mercaptoethylpyridine) Hypercel, for the validation of the simulation results. The adsorbent with adsorbed lysozyme is incubated in the elution buffer of different pH values, and then the elution efficiency is calculated as a function of pH. The protein conformational transition is evaluated by activity assay and fluorescence analysis. The effect of pH in HCIC is elucidated based on both the simulation and experimental results, which would be beneficial to the parameter optimisation for high-performance HCIC.

2. Model and simulation method

2.1 Protein model

The 46-bead β-barrel coarse-grained model protein [25] was used in the simulation. In this simplified mode, all residues are treated as spherical beads of equal size, connected by covalent bonds, with a bond length of 0.38 nm. The side chains are not explicitly considered. This model protein contains 46 beads which are divided into three groups and denoted as hydrophobic (H), hydrophilic (P) and neutral (N). The sequence is $H_9N_3(PH)_4N_3H_9N_3(PH)_5P$. The native structure of the model protein was obtained by the simulated annealing method. This model protein has both the hydrophobic core and exposed hydrophilic residues on the surface, and maintains its native structure by intra-molecular hydrophobic interaction. Therefore, this model protein can simulate the common properties of protein molecules. It has been extensively used to simulate the actual protein molecules in molecular simulations of protein folding [26,27] and aggregation [28,29]. A charged state of this model protein was also defined, as described in an earlier work [24], to simulate the protein in desorption. In the charged state, all hydrophilic beads (P) carry charge +0.4 and are, thus, included in the calculation of Coulomb potential energy. It was verified by the simulated annealing method that the model protein retained its native structure in the charged state, but has a flatter conformation (data not shown). The details of the model protein are described in the Supplementary Material, available online.

2.2 HCIC adsorbent pore model

The coarse-grained ligand model consists of two hydrophobic beads, H1 and H2, and a hydrophobic chargeable bead, HQ, at the end. It was constructed to simulate MEP (pK_a 4.85). The details of the ligand model are described in the Supporting Information. The ligands were then immobilised on the interior surface of a cylinder with infinite length to simulate the HCIC adsorbent pore. The average ligand density on the pore surface was 2.212 μmol/m^2 in the present study. The charge number on bead HQ was calculated from Equation (1) to simulate the change of pH of the mobile phase. Herein, the charge number was reduced by a factor of 0.4 to get stable simulation, with the final values listed in Table 1.

$$Q = \frac{10^{(pKa-pH)}}{1+10^{(pKa-pH)}}, \quad (1)$$

where Q is the charge number; pK_a is the pH when 50% of the ligands are charged.

2.3 Simulation methods

The Langevin dynamics and NVT ensemble were performed to examine the protein conformational transition within the HCIC adsorbent pore, according to the procedure proposed in a previous work [24]. Gromacs 3.3.3 [30,31] was used as the platform. Simulation box was prepared as previous simulations [24]. MD simulations of 100 ns were then performed to obtain 25 stably bound conformations of model proteins. This set of structures was used for 50 ns simulations of desorption at different pH values. Starting from the stably bound state, the charge on hydrophilic beads in protein was adjusted to +0.4, and the charge on bead HQ in ligands was adjusted to the number listed in Table 1 to promote the desorption process. All snapshots were prepared using the Rasmol program [32].

Two key parameters were calculated during the courses of simulations: the protein's radius of gyration (R_g) and the structural overlap function (χ), as described in

Table 1. Charge number of bead HQ in ligands at various pH values of the mobile phase.

pH	Charge number
3.00	0.394
4.00	0.350
5.00	0.166
6.00	0.026
7.00	0.003

the previous studies [33,34]. Protein conformation was then quantitatively distinguished by these two parameters, including the native (N), intermediate (M) and unfolded (U) states defined by Formula (S4) of the Supplementary Material, available online. The molar fraction was denoted as *f*. For instance, f_U was the fraction of the unfolded state. To examine the adsorption behaviour of the protein, the stable adsorption state (B) and desorption state (D) were defined by Formula (S6). Then, the desorption probability from simulation $P_{D,sim}$ was defined by

$$P_{D,sim} = \frac{1}{M_T} \sum_{i=1}^{M_T} \frac{t_{Di}}{t_{sim}}, \quad (2)$$

where M_T is the total number of trajectories; t_{Di} is the desorption lifetime in each trajectory; and t_{sim} is the total simulation time.

More details are given in the Supplementary Material, available online.

3. Experiments

3.1 Materials

Hen egg white lysozyme (14.3 kDa, p*I* 11.1) and *Micrococcus lysodeikticus* were purchased from Sigma (St Louis, MO, USA). Trishydroxymethylaminomethane (Tris) was from Promega (Fitchburg, WI, USA). MEP Hypercel was received from Pall Life Sciences (New York, USA). All other reagents were of analytical grade from local sources.

3.2 Adsorption

Lysozyme adsorption to MEP Hypercel was performed by finite batch adsorption experiments at pH 7.10. MEP Hypercel was washed with deionised water, followed by pre-equilibration in 0.01 mol/l Tris–HCl buffer (pH 7.10) plus 0.01 mol/l NaCl (buffer A). It was then filtered on a G3 sintered glass funnel. The density of MEP Hypercel was determined to be 1.072 ± 0.006 g/ml by a pycnometer. After pre-equilibration, 0.1 g of the wet adsorbent and 5.0 ml buffer A containing 2.0 mg/ml protein were added into 50 ml Erlenmeyer flasks, followed by shaking for 24 h in a water bath at 25°C. The solutions in the flasks were then centrifuged at 4000 rpm for 10 min. The protein concentration in the supernatant was determined by a UV–vis spectrometer at 280 nm (Perkin-Elmer, Shelton, CT, USA). The amount of the adsorbed protein on the adsorbent was then calculated by mass balance:

$$q = \frac{(c_0 - c) \times V_L}{V_S}, \quad (3)$$

where q and c are the equilibrium concentrations of the protein in the solid and liquid phase, respectively; c_0 is the initial protein concentration in the liquid phase; V_S and V_L are the volume of the solid phase and the liquid phase, respectively.

3.3 Elution

The adsorbent with adsorbed protein obtained above was incubated in the elution buffer for elution. The elution buffer used in the present study was 0.05 mol/l citric acid–disodium hydrogen phosphate buffers of pH 3.0, 4.0, 5.0, 6.0 and 7.0. Similar to the procedure in adsorption, 0.1 g of the wet adsorbent and 5.0 ml elution buffer were added into 50 ml Erlenmeyer flasks, followed by shaking for 24 h in a water bath at 25°C. The solutions in the flasks were then centrifuged at 4000 rpm for 10 min. The protein concentration in the supernatant was also determined by UV absorbance at 280 nm. The elution efficiency $P_{D,exp}$ was then calculated by:

$$P_{D,exp} = \frac{c \times V_L}{q \times V_S}. \quad (4)$$

Two parallel elution experiments were carried out, and the average elution efficiency value was used.

3.4 Lysozyme activity assay

Lysozyme activity was examined using *M. lysodeikticus* as the substrate dispersed in 0.1 mol/l sodium phosphate buffer (pH 6.24) at a concentration of 0.25 mg/ml [35]. The assay volume was 1.5 ml containing a 0.25 ml protein sample. Lysozyme samples were diluted to around 0.01 mg/ml prior to the assay. The decrease in the absorbance of the mixed solution at 450 nm was then recorded during the first 1.5 min at a frequency of 15 s. The relative activity of a sample was expressed in percentage of activity with respect to that of the native lysozyme measured at the same condition. Each sample was measured three times and the average of the three results was used.

3.5 Fluorescence spectroscopy

Fluorescence spectrum of lysozyme was obtained by exciting the protein solution at 280 nm and recording the emission spectra from 300 to 500 nm using a LS55 luminescence spectrometer (Perkin-Elmer). Each sample was measured three times and the average of the three results was used for analysis. The peak value and position of emission spectra were analysed to evaluate the compactness of the protein tertiary structure. The ratio of fluorescence emission intensity at 340 nm to that at 350 nm, denoted as F_{340}/F_{350}, is calculated to evaluate the fraction of native lysozyme in a sample [36,37].

4. Results and discussion

4.1 Elution efficiency

Elution efficiency is a key parameter to evaluate the recovery in HCIC. Herein, desorption probability, $P_{D,sim}$, is

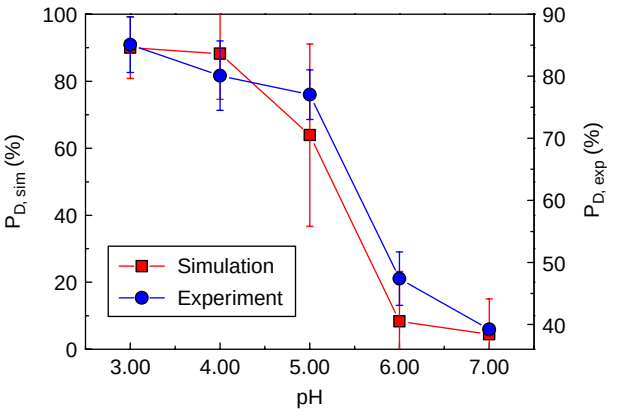

Figure 1. Elution efficiency as a function of pH of the mobile phase: (-■-) simulation and (-●-) experimental results. The error bars in simulation results indicate the standard deviations of 25 independent simulations, while the error bars in experimental results indicate the standard deviations of two parallel experiments.

calculated from the simulation results at all pH values, as shown by the red line in Figure 1, where the error bars indicate the standard deviations of 25 independent simulations (colour online).

It can be seen that $P_{D,sim}$ decreases with increasing pH in a non-linear manner. A mild decrease is observed at pH ranges of 3.0–4.0 and 6.0–7.0, while a sharp decrease is observed around pH 5.0. The analysis on the protein–ligand interaction provides a reasonable elucidation. The dominant driving force is electrostatic repulsion between the protein and ligands at low pH, leading to stable desorption. At neutral pH, however, the dominant driving force shifts to hydrophobic interaction, leading to stable adsorption. However, around pH 5.0, there is a balance between the electrostatic repulsion and the hydrophobic adsorption, leading to an unstable state of the protein between adsorption and desorption. This is indicated by the large error bar.

Experiments were performed for validation of the simulation results. The elution efficiency $P_{D,exp}$ was calculated and is shown by the blue line in Figure 1 (colour online). The error bars indicate the standard deviations between two parallel experiments. Because it is difficult to find an actual protein with a β-barrel structure (structure model of the protein used in simulations) for the experiment, lysozyme is chosen as the model protein instead.

Figure 1 shows that the simulation and experimental results are qualitatively consistent, indicating the reliability of simulation results. Although the protein used in simulation is an idealised model with a different structure from lysozyme, it has both the hydrophobic core and exposed hydrophilic residues on the surface. This is the common properties of protein molecules also revealed in lysozyme. Moreover, because the elution is driven by the strong repulsion between the protein and ligands, the parameter set used in the present study can simulate the inter-molecular interaction correctly and, thus, gives qualitatively consistent results. $P_{D,exp}$ decreases with increasing pH, indicating that low pH is favourable for elution. Most of the captured lysozyme in MEP Hypercel can be dissociated at pH < 5.0. The elution efficiency goes up to 90% at pH 3.0. It should be noted that the elution efficiency cannot reach 100% in the finite batch experiment due to the protein partitioning between the bulk liquid phase and the adsorbent pores. For the same reason, the elution efficiency cannot drop to 0 at a higher pH value due to the moderate binding strength of lysozyme to the adsorbent [38]. So, at pH 7.0, an elution efficiency as high as 40% is observed. This is expected from the adsorption isotherm at this pH value (data not shown).

4.2 *Protein conformational transition*

Protein conformational transition is crucial for the yield of native protein and, thus, the quality of purification products. As mentioned above, high elution efficiency is observed at acidic conditions. However, the acidic pH is deviated from the optimum pH of the protein, and the loss of protein activity may occur. To evaluate the protein conformational transition within the adsorbent pores, the protein fractions of different states were calculated. The simulated native fraction f_N and unfolded fraction f_U at all pH values are shown in Figure 2(a), while the native yield determined experimentally by enzymatic activity and fluorescence assay are shown in Figure 2(b) and Table 2, respectively.

The simulation results show that f_N is small at all pH values, with a maximum of 28.1% at pH 3.0. This indicates that the elution environment is harmful for the preservation of the native protein conformation. Figure 2(a) also shows that f_N decreases and f_U increases with increasing pH. The f_U reaches the maximum, 52.5%, at pH 6.0 and then slightly decreases to 49.1% at pH 7.0.

However, Figure 2(b) reveals that the protein activity is always larger than 100% and shows little difference at different pH values. It can be seen that the error bars are small except in pH 6.0, indicating good reproducibility of the experimental data. The reference state in the present study to calculate the specific activity is freshly prepared commercial lysozyme purchased from Sigma (purity $\geq$ 90% as given in the products catalogue). So, the recovery of enzymatic activity higher than 100% may be due to the presence of impurities and minor denatured proteins in the commercial lysozyme sample. The impurities, for example albumin, may remain adsorbed under the eluting condition because it is an acidic protein (isoelectric point, 4.7). Meanwhile, the denatured protein may keep binding in the elution due to its stronger hydrophobicity. Therefore, the eluted lysozyme from the HCIC adsorbent is purified, leading to higher enzymatic activity as compared with the reference state. However, it should be noted that there is no

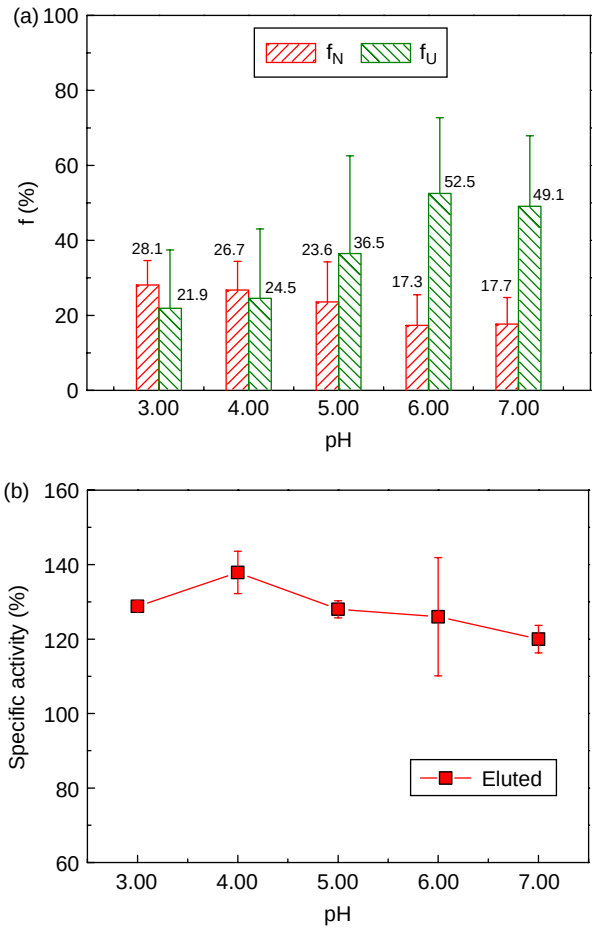

Figure 2. The protein fractions of different conformations in simulation (a) and specific activity after elution in experiment (b). The error bars have the same meaning as in Figure 1.

Table 2. Fluorescence analysis of lysozyme eluted at various pH values of the mobile phase.

pH	Peak value	Peak position	F_{340}/F_{350}
3.00	125.2 (5.2[a])	343.5 (2.1)	0.872 (0.000)
4.00	119.4 (0.5)	344.0 (0.7)	0.874 (0.008)
5.00	134.5 (12.4)	342.8 (0.4)	0.866 (0.006)
6.00	163.0 (27.6)	343.8 (0.4)	0.865 (0.003)
7.00	188.7 (8.9)	344.3 (1.1)	0.857 (0.001)

[a] The number in parentheses indicates the standard deviation in duplicate experiments.

significant difference of protein activity at different pH values. It can then be concluded that protein activity is independent of the pH of the elution buffer. To further verify the results, the fluorescence data of the eluted protein samples were examined and are shown in Table 2.

A red shift in the emission maximum is observed in comparison with the native state (340.0 nm, determined with the fresh native lysozyme). However, the shift value is small and there is no remarkable difference at different pH values. In addition, the ratio F_{340}/F_{350} decreases with increasing pH, but the extent is still very small. Therefore, the experimental results indicate that the protein activity and structure kept unchanged at the elution conditions with different pH values. This difference between the simulation and experimental results will be elucidated below.

4.3 Microscopic information of the elution process

The elution process is examined by the MD simulation to provide microscopic information of the process within the adsorbent pores. The dynamic trajectories and representative snapshots at various pH values are shown in Figures 3–5, where the time courses of χ, R_g, d and E are shown in (a) and the snapshots at the time points marked in (a) are shown in (b).

At the initial stage (0.74 ns) at pH 3.0, the coexisting forces of hydrophobic adsorption on the hydrophobic beads and electrostatic repulsion on the hydrophilic beads of the protein lead to the extension of the protein structure, indicated by the large χ and R_g values. Because the electrostatic repulsion (purple curve) is stronger than the hydrophobic attraction (green curve), the protein moves away from the ligands (colour online). At 15.44 ns, transitory unfolding is observed. At 23.33 ns, both χ and R_g values decrease, indicating restoration of the native structure by the intra-molecular hydrophobic interaction. At 40.0 ns, the protein is parallel to the ligand surface, but the chain rich in hydrophilic beads contacts with the ligands, so the protein is repulsed away. At 46.44 ns, the protein–ligand distance continues to increase. The protein then keeps the state of completely dissociated state until the end of the simulation. The elution process at pH 4.0 is similar to that at pH 3.0 (data not shown).

At pH 5.0, however, the situation is somewhat different (Figure 4). The initial stage shows no remarkable differences from that at pH 3.0. At 40.0 ns, however, the protein approaches the ligands and the hydrophobic beads contact with the ligands. This is clearly indicated by the remarkable increase in the hydrophobic interaction energy (green curve, colour online). At the same time, electrostatic repulsion on the hydrophilic beads is observed, leading to significant protein unfolding. After that, the protein remains in the adsorbed state until the end of the simulation.

At pH 6.0 (Figure 5), the trajectories show that the hydrophobic interaction is always the dominant driving force. Namely, the stably bound state is almost maintained. At 0.74 ns, the protein is unfolded at the adsorbed state. At 15.44 ns, the protein dissociates from the ligands temporarily. However, because of the presence of strong hydrophobic interaction, the protein returns to the stably bound state at 23.33 ns, with the hydrophobic patch stably bound on the ligands. Here, the hydrophilic beads move to the bulk fluid due to the electrostatic repulsion, leading to serious unfolding, as

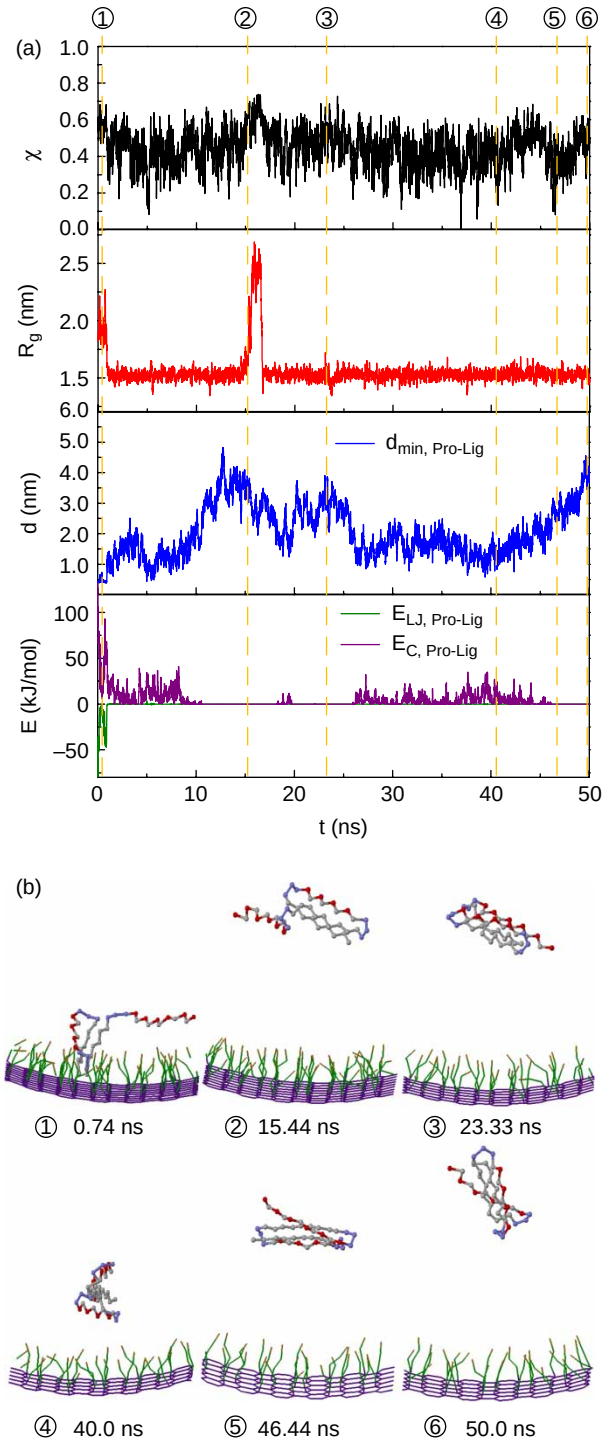

Figure 3. Desorption behaviour at pH 3.0. The time courses of χ, R_g, d and E in desorption trajectory are shown in (a), and the corresponding snapshots at the time points marked in (a) are shown in (b).

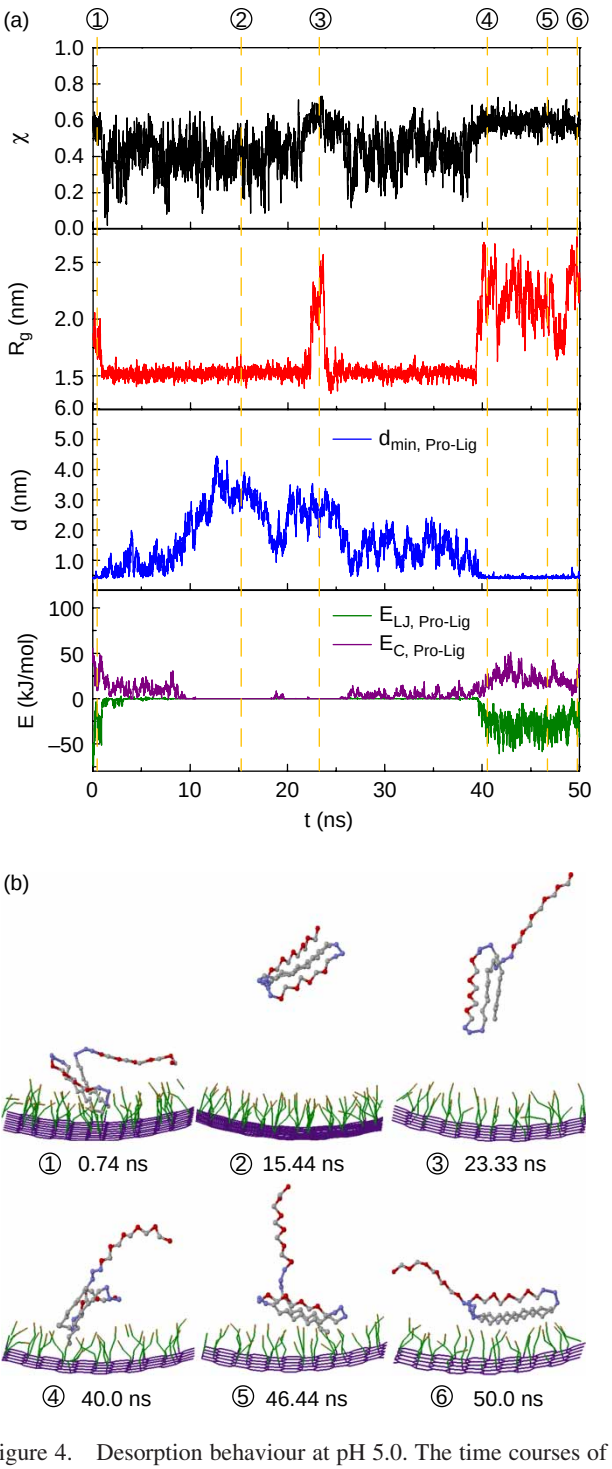

Figure 4. Desorption behaviour at pH 5.0. The time courses of χ, R_g, d and E in desorption trajectory are shown in (a), and the corresponding snapshots at the time points marked in (a) are shown in (b).

indicated by the large χ and R_g values. At 40.0 ns, the protein retains its native structure. However, unfolding is observed once again at 46.44 ns.

At pH 7.0, because the ligand carries little charge, protein–ligand electrostatic interaction energy is very small (data not shown). The protein, thus, keeps bound on the ligand surface, with serious unfolding.

Therefore, at neutral pH, the protein remains on the ligand surface and, thus, suffers from serious unfolding. For further verification, the distributions of the unfolded

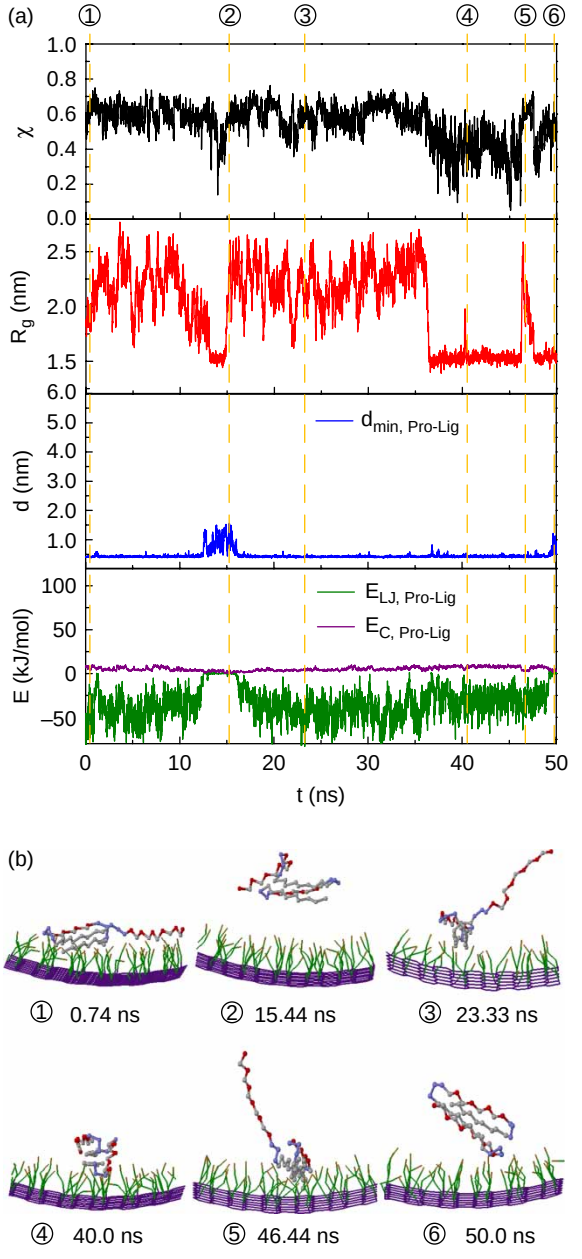

Figure 5. Desorption behaviour at pH 6.0. The time courses of χ, R_g, d and E in desorption trajectory are shown in (a), and the corresponding snapshots at the time points marked in (a) are shown in (b).

protein within the pore at all pH values are calculated and shown in Figure 6.

At pH 3.0–5.0, an obvious peak of the unfolded protein fraction at the protein–ligand distance 1.7 nm (bulk liquid phase) is observed. At pH 6.0 and 7.0, however, the peak in the bulk liquid disappears, and only a peak on the ligand surface is observed. The peak value on the ligand surface increases with the pH of the mobile phase. Therefore, at low pH, most of the unfolded proteins exist in the bulk liquid, which is caused by the long-range

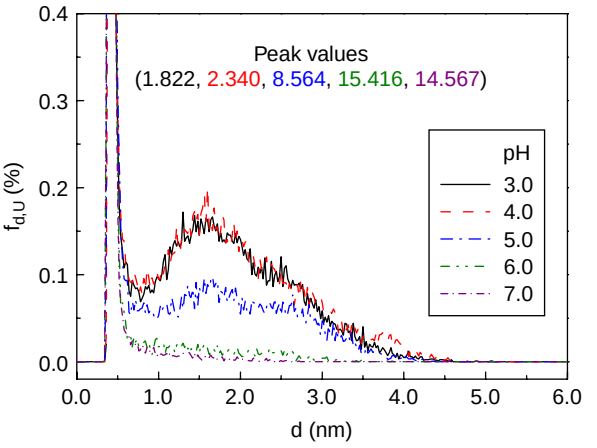

Figure 6. Unfolded protein distributions within the adsorbent pore in desorption at various pH values. Peak values are provided in the inset with coloured numbers (colour online).

electrostatic interaction. At neutral pH, protein unfolding mainly occurs on the adsorbent surface due to the presence of simultaneous hydrophobic attraction and electrostatic repulsion from the ligands.

It is then concluded that the difference between the simulation and experimental results is caused by different locations of the detected protein. In the experiment, both the enzymatic and fluorescence assay can only detect the protein in the bulk liquid. However, most of the protein unfolding occurs on the ligand surface or its vicinity, as has been revealed by the simulations (Figure 6). Thus, different positions for examination result in the deviation about the protein conformational transition between the simulation and experimental results.

5. Conclusions

Molecular dynamics simulation was performed to investigate the effect of pH on elution efficiency and conformational transition of a 46-bead β-barrel coarse-grained model protein within an HCIC coarse-grained adsorbent pore. The elution of lysozyme in MEP Hypercel was also conducted to examine the elution efficiency and preservation of protein activity at various pH values. The simulations show that elution efficiency decreases with increasing pH in a non-linear manner, which is qualitatively consistent with the experimental results. Large fluctuations are observed around pH 5.0 due to the balance between the electrostatic repulsion and the hydrophobic attraction. Protein conformational transition shows that at low pH, the protein is dissociated quickly due to strong electrostatic repulsion, and only a small fraction of the protein is unfolded. At neutral pH, the protein keeps bound on the ligand surface, and the simultaneous hydrophobic attraction and electrostatic repulsion causes serious protein unfolding. However, this is different from the experimental results, where the activity and fluorescence spectra of lysozyme are

independent of pH. This difference has been explained by the difference in sample positions for examination. That is, only the protein in the bulk liquid can be detected in the experiments. Therefore, the effect of pH in HCIC has been elucidated based on both the simulation and experimental results. It would be beneficial to the parameter optimisation for high-performance HCIC.

Acknowledgements

This work was supported by the Natural Science Foundation of China (Nos 20636040 and 20976126) and the China Postdoctoral Science Foundation (No. 20080440679).

References

[1] S.C. Burton and D.R. Harding, *Hydrophobic charge induction chromatography: Salt independent protein adsorption and facile elution with aqueous buffers*, J. Chromatogr. A 814 (1998), pp. 71–81.

[2] W. Schwartz, D. Judd, M. Wysocki, L. Guerrier, E. Birck-Wilson, and E. Boschetti, *Comparison of hydrophobic charge induction chromatography with affinity chromatography on protein A for harvest and purification of antibodies*, J. Chromatogr. A 908 (2001), pp. 251–263.

[3] M.P. Dux, R. Barent, J. Sinha, M. Gouthro, T. Swanson, A. Barthuli, M. Inan, J.T. Ross, L.A. Smith, T.J. Smith, R. Webb, B. Loveless, I. Henderson, and M.M. Meagher, *Purification and scale-up of a recombinant heavy chain fragment C of botulinum neurotoxin serotype E in* Pichia pastoris *GS115*, Protein Expres. Purif. 45 (2006), pp. 359–367.

[4] G.T. Weatherly, A. Bouvier, D.D. Lydiard, J. Chapline, I. Henderson, J.L. Schrimsher, and S.R. Shepard, *Initial purification of recombinant botulinum neurotoxin fragments for pharmaceutical production using hydrophobic charge induction chromatography*, J. Chromatogr. A 952 (2002), pp. 99–110.

[5] L. Guerrier, P. Girot, W. Schwartz, and E. Boschetti, *New method for the selective capture of antibodies under physiological conditions*, Bioseparation 9 (2000), pp. 211–221.

[6] L. Guerrier, I. Flayeux, and E. Boschetti, *A dual-mode approach to the selective separation of antibodies and their fragments*, J. Chromatogr. B 755 (2001), pp. 37–46.

[7] E. Boschetti, *Antibody separation by hydrophobic charge induction chromatography*, Trends Biotechnol. 20 (2002), pp. 333–337.

[8] G.F. Zhao and Y. Sun, *Displacement chromatography of proteins on hydrophobic charge induction adsorbent column*, J. Chromatogr. A 1165 (2007), pp. 109–115.

[9] S. Ghose, B. Hubbard, and S.M. Cramer, *Evaluation and comparison of alternatives to protein A chromatography – Mimetic and hydrophobic charge induction chromatographic stationary phases*, J. Chromatogr. A 1122 (2006), pp. 144–152.

[10] D. Coulon, C. Cabanne, V. Fitton, A.M. Noubhani, E. Saint-Christophe, and X. Santarelli, *Penicillin acylase purification with the aid of hydrophobic charge induction chromatography*, J. Chromatogr. B 808 (2004), pp. 111–115.

[11] G.F. Zhao, G.Y. Peng, F.Q. Li, Q.H. Shi, and Y. Sun, *5-Aminoindole, a new ligand for hydrophobic charge induction chromatography*, J. Chromatogr. A 1211 (2008), pp. 90–98.

[12] D. Frenkel and B. Smit, *Understanding Molecular Simulation: From Algorithms to Applications*, 2nd ed., Academic Press, San Diego, CA, 2002.

[13] L. Zhang and Y. Sun, *Molecular simulation of adsorption and its implications to protein chromatography: A review*, Biochem. Eng. J. 48 (2009), pp. 408–415.

[14] A.R. Bizzarri, G. Costantini, and S. Cannistraro, *MD simulation of a plastocyanin mutant adsorbed onto a gold surface*, Biophys. Chem. 106 (2003), pp. 111–123.

[15] J.C. Hower, Y. He, and S.Y. Jiang, *A molecular simulation study of methylated and hydroxyl sugar-based self-assembled monolayers: Surface hydration and resistance to protein adsorption*, J. Chem. Phys. 129 (2008), 215101–215107.

[16] R.A. Latour, *Molecular simulation of protein–surface interactions: Benefits, problems, solutions, and future directions*, Biointerphases 3 (2008), pp. FC2–FC12.

[17] A.A. Mungikar and D. Forciniti, *Computer simulations and neutron reflectivity of proteins at interfaces*, Chemphyschem 3 (2002), pp. 993–999.

[18] G. Raffaini and F. Ganazzoli, *Understanding the performance of biomaterials through molecular modeling: Crossing the bridge between their intrinsic properties and the surface adsorption of proteins*, Macromol. Biosci. 7 (2007), pp. 552–566.

[19] K.B. Lipkowitz, *Atomistic modeling of enantioselection in chromatography*, J. Chromatogr. A 906 (2001), pp. 417–442.

[20] A. Felinger, *Molecular dynamic theories in chromatography*, J. Chromatogr. A 1184 (2008), pp. 20–41.

[21] V. Daggett, *Long timescale simulations*, Curr. Opin. Struct. Biol. 10 (2000), pp. 160–164.

[22] V. Daggett, *Protein folding-simulation*, Chem. Rev. 106 (2006), pp. 1898–1916.

[23] M. Karplus and J.A. McCammon, *Molecular dynamics simulations of biomolecules*, Nat. Struct. Biol. 9 (2002), pp. 646–652.

[24] L. Zhang, G.F. Zhao, and Y. Sun, *Molecular insight into protein conformational transition in hydrophobic charge induction chromatography: A molecular dynamics simulation*, J. Phys. Chem. B 113 (2009), pp. 6873–6880.

[25] J.D. Honeycutt and D. Thirumalai, *Metastability of the folded states of globular proteins*, Proc. Natl Acad. Sci. USA 87 (1990), pp. 3526–3529.

[26] T. Veitshans, D. Klimov, and D. Thirumalai, *Protein folding kinetics: Timescales, pathways and energy landscapes in terms of sequence-dependent properties*, Fold. Des. 2 (1997), pp. 1–22.

[27] Z.Y. Guo, D. Thirumalai, and J.D. Honeycutt, *Folding kinetics of proteins – A model study*, J. Chem. Phys. 97 (1992), pp. 525–535.

[28] T. Cellmer, D. Bratko, J.M. Prausnitz, and H. Blanch, *The competition between protein folding and aggregation: Off-lattice minimalist model studies*, Biotechnol. Bioeng. 89 (2005), pp. 78–87.

[29] H.B. Jang, C.K. Hall, and Y.Q. Zhou, *Assembly and kinetic folding pathways of a tetrameric beta-sheet complex: Molecular dynamics simulations on simplified off-lattice protein models*, Biophys. J. 86 (2004), pp. 31–49.

[30] H.J. Berendsen, D. Vanderspoel, and R. Vandrunen, *Gromacs – A message-passing parallel molecular-dynamics implementation*, Comput. Phys. Commun. 91 (1995), pp. 43–56.

[31] E. Lindahl, B. Hess, and D. van der Spoel, *GROMACS 3.0: A package for molecular simulation and trajectory analysis*, J. Mol. Model. 7 (2001), pp. 306–317.

[32] R. Sayle and E. Milnerwhite, *RASMOL – Biomolecular graphics for all*, Trends Biochem. Sci. 20 (1995), pp. 374–376.

[33] L. Zhang, D.N. Lu, and Z. Liu, *Dynamic control of protein conformation transition in chromatographic separation based on hydrophobic interactions: Molecular dynamics simulation*, J. Chromatogr. A 1216 (2009), pp. 2483–2490.

[34] D.N. Lu and Z. Liu, *Oscillatory molecular driving force for protein folding at high concentration: A molecular simulation*, J. Phys. Chem. B 112 (2008), pp. 2686–2693.

[35] D. Batas and J.B. Chaudhuri, *Protein refolding at high concentration using size-exclusion chromatography*, Biotechnol. Bioeng. 50 (1996), pp. 16–23.

[36] H.N. Ong, B. Arumugam, and S. Tayyab, *Succinylation-induced conformational destabilization of lysozyme as studied by guanidine hydrochloride denaturation*, J. Biochem. 146 (2009), pp. 895–904.

[37] M. Van Der Veen, W. Norde, and M.C. Stuart, *Effects of succinylation on the structure and thermostability of lysozyme*, J. Agric. Food Chem. 53 (2005), pp. 5702–5707.

[38] S. Ghose, B. Hubbard, and S.M. Cramer, *Protein interactions in hydrophobic charge induction chromatography (HCIC)*, Biotechnol. Progr. 21 (2005), pp. 498–508.